Engineering Science and Technology, an International Journal 46 (2023) 101505

Contents lists available at ScienceDirect

Engineering Science and Technology, an International Journal

journal homepage: www.elsevier.com/locate/jestch

The Effect of Conducted Emissions of Grid-Tied Three-Phase Adjustable Drives

Secil Genc [a,*], Venkatkumar Muneeswaran [b], David Thomas [b], Steve Greedy [b], Burcu Gundogdu [c], Nur Sarma [d,e], Okan Ozgonenel [a]

[a] Ondokuz Mayis University, Electrical Electronics Engineering Department, Samsun, Turkey
[b] University of Nottingham, Electrical Electronics Engineering Department, Nottingham, UK
[c] Hakkari University Colemerik, VHS, Computer Technologies, Hakkari, Turkey
[d] Duzce University, Electrical Electronics Engineering Department, Duzce, Turkey
[e] Durham University, Department of Engineering, Durham, UK

ARTICLE INFO

Keywords:
Conducted emission (CE)
Electromagnetic compatibility (EMC)
Electromagnetic interference (EMI)
Adjustable motor drive inverters

ABSTRACT

Electromagnetic Interference (EMI) is generated and mitigated in power converters. EMI problems are related to high-speed power converters. This article focuses on conducted electromagnetic interference in adjustable-speed drive (ASD) systems. The electromagnetic compatibility of three-phase/level grid-connected drive inverters is investigated. The test setup is built per the CISPR16-1–2 standard, and the interferences produced from the inverter to the grid are measured. The main dependencies of conducted emissions of a power inverter, changes in the length/shape of main cables, and motor speed have been investigated under load and no load conditions. Factors affecting EMI performance and filter design issues will be addressed. A statistical approach to quantifying the frequency domain impact of conducted emission noise created on the three-phase system by operating various emission sources. Fast Fourier Transform (FFT) was applied for time–frequency domain conversion, and to evaluate with a statistical approach Minitab software was used. Then, a filter design is created to prevent these interferences from being conducted to the grid. Also, the noise attenuation of the EMI filter has been validated in the simulation. Briefly, this study fills in the blanks of uncertainties involved in measuring three-phase emissions, which helps the engineers at the design stage of three-phase converters.

1. Introduction

The advancement of the power electronic converter can be seen in different industries, including automotive, aerospace, and power distribution, as it imposes new criteria for better power density, higher switching frequency, and improved efficiency. With increased electrification, the use of power electronics in automobile safety–critical applications grows more extensive. The device's electromagnetic compatibility is challenged by the need for higher power density and better controllability [1].

EMC is a critical component in the design of any power electronic equipment [2]. The main source of electromagnetic emission in the main ports of adjustable-speed electrical power drive systems is pulse width modulation (PWM) switching. Pulse rise and fall times are now less than 200 ns in power systems, making them a significant source of conducted (0.15–30 MHz) and radiated (30 MHz-1 GHz) emissions [1–3]. EMI is an undesired effect caused by electromagnetic radiation or electromagnetic conduction from a device [4–6], and the management of which is called EMC. Power quality (PQ) has traditionally dealt with low frequencies up to 2 kHz. The PQ is described as the properties of electric current, voltage, and frequency at a specific place in an electric power system when compared to a set of reference technical parameters or standards. There is a spectral gap between these two well-known frequency ranges [7–11], as shown in Figure 1. Indeed, standards for this intermediate band need to be improved. However, the lack of standards in this frequency range does not indicate that it is free of EMI.

This spectral gap is directly related to technological advancement. At the same time, The European Committee for Electrotechnical Standardization (CENELEC) has already issued two reports on this subject. They agreed to keep IEC 61000–2-2 and IEC 61000–2-12 standards to establish compatibility levels between 2 and 150 kHz [12].

The standard IEC 61000–2-2 was recently updated to allow the

* Corresponding author.
E-mail address: secil.yilmaz@omu.edu.tr (S. Genc).

https://doi.org/10.1016/j.jestch.2023.101505
Received 3 April 2023; Received in revised form 17 July 2023; Accepted 3 August 2023
Available online 16 August 2023

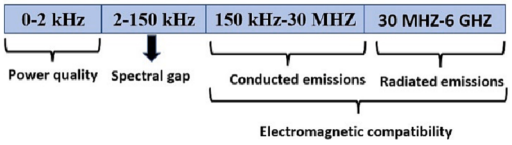

Fig. 1. Split the frequency spectrum into the range of frequencies [7].

2–150 kHz frequency range. However, emission limitations are now described separately. Standardization organizations are actively establishing standards for this frequency range. In this study, new measures have been recommended associated with emissions in the frequency range of 9–150 kHz [13]. Furthermore, changes across test sites may affect measurement repeatability in the EMC framework. Different setup conditions, such as table positioning [14], length, height, manner of main cable meandering, and the positioning of the equipment under test, may influence conducted emission measurements. Unfortunately, there is freedom for conducted emissions test methods regarding cable positioning, table material, and table positioning, introducing additional sources of systematic error and uncertainty. To be reliable in determining if a product meets or does not meet EMC regulations, this evaluation must take into account the criteria indicated above related [1]. EMI noise must be provided to the filter designer to design an effective filter. This information can be obtained either through history or actual measurement. For products with history, estimating the baseline EMI noise is more accessible, and the data must be received by measurement. The purpose of this study is to evaluate and measure the conducted emissions produced by variable-speed electrical power drive systems under load and no load conditions. Issues related to the cable connecting the power source and the three-phase converter playing a crucial role in CE have been investigated in some studies [15–20]. These studies focus on the following issues: Wershoven [15] and Pahl [16] reported CE emissions regarding cable length at frequencies over 150 kHz; however, they did not evaluate them according to standards. Sergio et al. have investigated long-cable effects on CE analytically [17]. Santos et al. evaluated unshielded cable models and length using EMI simulations instead of an experimental setup [20]. Marshall has reported the effect of the cable bundling over CE up to 120 MHz [19]. Benazza has investigated the cable effect for DC systems [18]. Among them, the relevance of CE in ASD systems has been addressed in [21–22]. In [23], Luszcz evaluated the emissions AC motor and fed the AC motor with cable. However, different cable lengths were not assessed and covered the 150 kHz -30 MHz frequency range. Moreau et al. compared the simulation and measurement of CE results from systems achieved up to 50 MHz without standards [21]. Daniele et al. reported emissions produced by a variable speed drive applied to an electrical load in the frequency range of 150 kHz to 30 MHz, but no standards have also been defined [22]. An overview of proposed measures is given in this study: CISPR 11 standard specifies emission limits for scientific, medical, or industrial equipment; CISPR 15 standard specifies emission limits for electrical lighting systems and is at the same emission limits as the CISPR 11 standard, but generally includes higher frequency ranges; IEC TS 62578 standard explain the operating conditions and characteristics of active supply transducers; EN50065 general and EN50065 industrial (the last two vary after 100 kHz) for power line communication, and EN 50160 describes the properties of low, medium, and high voltage supplies, as well as voltage events and changes and Mil-Std 461 standards for military testing standards. In addition to this, even in the motor's output frequency region of 0 Hz, equipment under test (EUT) causes conducted emissions. Besides that, several studies have concentrated on the design of three-phase EMI filters to meet emission standards [24,25]. This study examines the EMI emission of a grid-connected adjustable drive system in the frequency range of 9 kHz to 150 kHz. The effect of circumstances on EMI is discussed. To offer a reference for the EMI test uncertainty in this band, statistical approaches are introduced. Worst-case EMI filters have also been developed for this band. However, the EMI filter design for ASD drivers for the 9–150 kHz frequency range has not been investigated based on these uncertainties and there is limited research available on this topic. In contrast to other recent works in the field, the contributions of this work on CE in three-phase systems are listed as follows:

- General studies on conducted emissions of adjustable three-phase speed drive systems mainly focus on the above 150 kHz frequency range.

Given this, research will help to understand the nature of CE generation and propagation in the 9–150 kHz frequency range because of LISN's configuration.

- This study provides a comprehensive analysis of various circumstance impacts for conducted emissions in terms of cable length, speed of the driver, and load condition, as there needs to be a study in the literature which investigates these issues comprehensively. As a result, this study fills the need for more detailed knowledge for analyzing EMI filters. Therefore, the presented research is essential for designing and developing power electronic converters.
- The effect of cable length, speed, and load conditions have yet to be studied in terms of statistical approximations to distinguish between conditions to predict specific design parameters.
- Together operation of ASD systems on CE has not been investigated and not compared in terms of limit standards. To prevent CE, a design procedure is given based on a simulation related to the 9–150 kHz frequency range. Design results are verified with simulation in the PSIM EMI design suite.

These contributions fill gaps in the current knowledge and provide essential insights for the design and development of power electronic converters, making the paper a valuable addition to the existing literature in this field. This paper is structured as follows: Section 2 explains the experimental study. The effects of cable length, shape, and speed of the driver under load and no-load conditions are discussed in Section 3. Additionally, the results of the experimental study are presented with a statistical approach in this section. Section 4, filter layout and filter element selection, have been addressed. In the last section, the obtained results are discussed and briefly summarized.

2. Experimental setup

An experimental system was designed to examine the effect of the conducted emissions of the grid-tied three-phase adjustable drive system. The test setup used to analyze the conducted emission is given in Figure 2(a) and the configuration is presented as a block diagram in Figure 2(b). It is composed of a line impedance stabilization network (LISN) characterized by the frequency range of 9 kHz to 30 MHz, a three-phase AC/AC converter, an induction motor, and three phase cables: one links up the LISN and the inverter and another connects the inverter to the motor (three conductors with different length and shape) is given in Figure 2(a). For load conditions, the rig consists of a 3-phase (3φ) 1.5 kW 4-pole caged induction motor connected to a similar rated powder brake unit to act as a load. Configurations of motors used in no-load and load conditions are given in Table 1. Using a high-speed Keysight oscilloscope, CE signals in the time domain have been captured with a 1 MHz sampling frequency.

Figure 3 shows the flowchart of the proposed measurements for conducted emissions caused by a three-phase AC/AC converter. To begin with, the conducted emissions were analyzed under two different conditions. Loaded and no-load conditions effects of cable and length have been considered. Besides, load impact over CE also has been investigated. The use of a traditional EMI receiver is common practice for RF-conducted emission measurements. In this study, it is aimed to

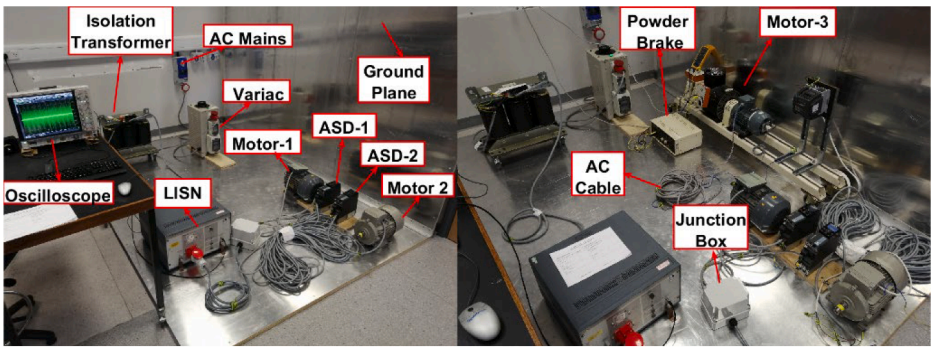

(a)

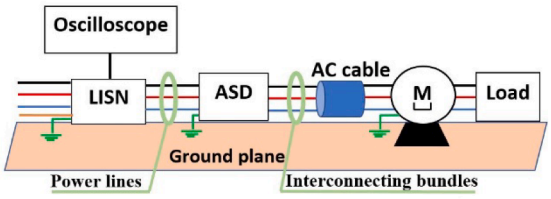

(b)

Fig. 2. Test setup of the experimental system (a) and block diagram of the experimental system (b).

Table 1
Configurations of motors.

B Motor Types	No Load Condition M1	 M2	Load Condition M3
Power(kW)	4	4	1.5
Frequency(F)	50	50	50
Nominal voltage (V)	400(Y)	230 V(Δ)	230 V(Δ)
Nominal Current(A)	8.1	13.8	6.5
Nominal Speed (rpm)	1460	2980	1435

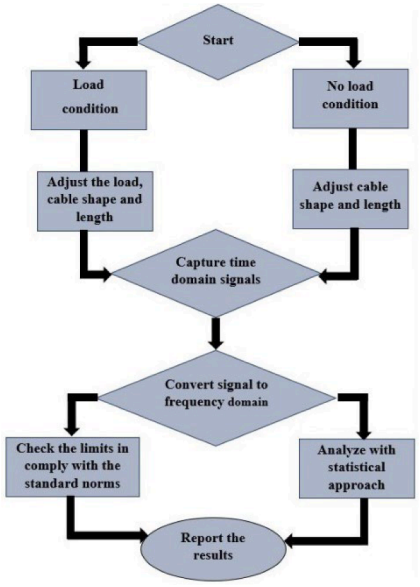

Fig. 3. Flowchart of the system.

compare the new standard limits that cover the frequency range of 9–150 kHz. Instead of using a physical receiver, a MATLAB algorithm based on FFT has been used as an alternative EMI receiver. For this purpose, the time-domain signal is captured with the oscilloscope. These disturbances have variable harmonic and amplitude properties throughout time. The frequency resolution has been taken as a 200 Hz band for collecting the signal in recommended EN 55065–1 standard, which covers 9–150 kHz frequency ranges. Then, this signal was converted to the frequency domain with FFT and compared to standard limits. Finally, the results were evaluated with a statistical approach to understand the differences between circumstances.

3. Evaluation of measurement uncertainties

3.1. *Various cable effect over CE*

A variable speed drive is a device that controls an electric motor by varying the constant voltage from the power supply to the desired amplitude and frequency. The motor is linked to the converter through an AC cable, contributing to parasitic capacitances and generating common mode current. To determine how connecting cables between the converter and motor affect EMI disturbances, 1 m, 10 m, 50 m, and 100 m cables were used. Firstly, background noise is set to ensure high accuracy and repeatability of the measurement. Figure 4 indicates that background noise is within acceptable limits according to the proposed standards measured from the L1 phase in a three-phase system.

The necessary noise attenuation calculation can easily be used to calculate suppression of a frequency range. The conducted emissions were measured for each phase under no-load conditions since the highest value of the needed noise is required for filter design. The outcome shown in Figure 5 indicates no significant difference in the CE for each phase. As a result, the L1 phase was chosen to measure CE.

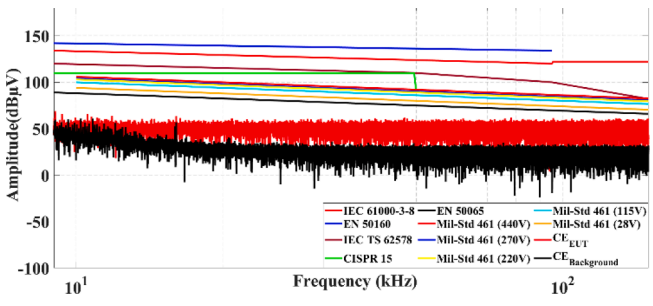

Fig. 4. The background noise level of the test environment.

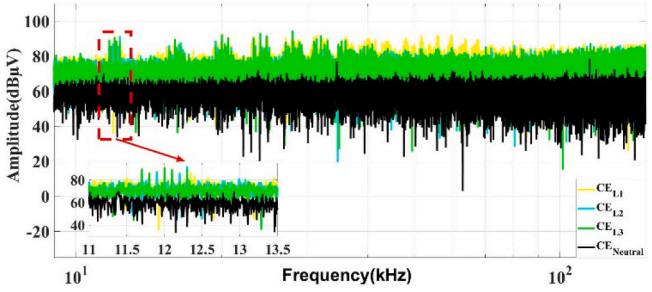

Fig. 5. Conducted emissions in each phase.

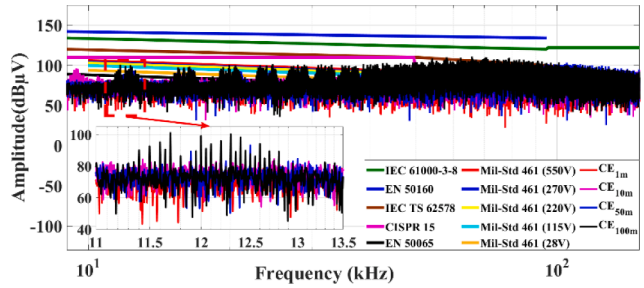

Fig. 6. EMI noise with various motor cable lengths.

Figure 5 shows CE is neutral under the limits, but L1, L2, and L3 phases exceed EN50065, MIL-STD standards.

The cable between the motor and converter influences the EMI disturbances. For this purpose, EMI noise with various motor cable lengths is given in Figure 6. The frequency resolution has been taken as a 200 Hz band for collecting the signal in recommended EN 55065–1 standard, which covers 9–150 kHz frequency ranges [26–27]. EMI noise with various motor cable lengths exceeds recommended standards except from IEC61000-3–8 and EN 50160. Statistical computations were employed to represent the experimentally acquired conducted emissions more effectively for this frequency range. Non-parametric statistical procedures such as the Kruskal Wallis and Mann-Whitney tests were employed as the experimental data did not follow a normal distribution. Furthermore, the Kruskal-Wallis test is used for multiple group comparisons.

In this approach, the probability of the test statistic appearing is compared to the alpha significance level set by the researcher, typically at 1% or 5%. The H, DF and P-values are measures used in statistical hypothesis testing. P represents the probability of obtaining a test statistic. It allows researchers to make decisions about the null hypothesis by comparing it to a predetermined significance level, often denoted as alpha (α). If the p-value is smaller than alpha, typically set at 0.05 or 0.01, it suggests that the observed data is unlikely to have occurred by chance alone, leading to the rejection of the null hypothesis (Ho). In this study, α is taken as 0.01. A smaller p-value indicates stronger evidence against the null hypothesis. H is the test statistic. The decision to reject the null hypothesis is made by comparing the test statistic, H, to a predetermined critical. Also, DF represents the degrees of freedom related to the test statistic, which is determined by the number of independent observations needed for its calculation and is equal to the number of groups minus one. The critical H value was determined to be 11.34 from the Kruskal Wallis table for a significance level of α =0.01. If the calculated test statistic is more significant than 11.34, the null hypothesis is rejected. It is concluded that there is a substantial difference between the groups being tested at the 0.01 level of significance. Suppose the calculated test statistic is less than or equal to 11.34. In that case, it failed to reject the null hypothesis and concluded that there was insufficient evidence to support the claim that there was a significant difference between the groups. The computed H test statistic for the

Table 2
Kruskal Wallis of cable length.

Groups	1 m	10 m	50 m	100 m
Median	70.3873	75.6239	76.5972	76.6743
Test statistics	DF=3, H=19059.21, P*=0.000			

P* <0.01 (α level of significance): The null hypothesis is rejected.

Kruskal-Wallis test is 19059.21, as given in Table 2. The null hypothesis is rejected because the test statistic value is much larger than this value. Also, the probability of this test statistic s evaluated as a P-Value occurring is nearly zero. Lower chances provide more substantial evidence against the null hypothesis. As a result, it is inferred that there is a difference in the medians of the groups, as given in Table 2.

The Mann-Whitney pairwise comparison test was then used to determine which groups had a difference in their medians. However, since the sample size (30001) is very large (>30), the test statistic was calculated using an effective sample test approach. In this case, the Mann-Whitney *U* test statistic follows a normal distribution and is transformed into Z-scores. These scores are also given in Table 3. At a significance level of 0.01, the critical value for Z-scores was 2.33 using the standard regular distribution table. As indicated by the results in Table 3, the Z scores are significantly larger than the critical value, meaning that the medians of all groups are different from each other.

The graphical plot is a popular method for visually presenting summary statistics. It has the advantage of conveying a large amount of information in a concise and easily understandable manner. Then, a visual method of Box plot and Main effect plot was utilized to find variations between groups, as shown in Figure 7. A box plot utilizes a box to indicate the location of the upper and lower quartiles, while the median is represented by the center of the box. The lower and upper quartiles represent the 25th and 75th percentiles of the distribution. The x-axis represents the parameter values, and the y-axis depicts the corresponding median response. The main effects plot illustrates how the mean response varies with different values of each length parameter, with the x-axis representing the parameter values and the y-axis showing the corresponding mean response. The horizontal line in the plot acts as a reference point, representing the average response across various levels or categories of the process parameters. This line helps in understanding the typical or average behavior of the response variable in relation to different values of the length parameters. These statistical approaches were used separately for each experimental group, and significant differences were found between groups. According to these results, there is a statistical difference between the lengths, and it is reported that the conducted emission is more significant when the cable

Table 3
Mann-Whitney Test for ASD-1 and ASD-2.

Groups	Statistics U	Statistics Z	P* Value
1 m-10 m	679,686,000	108.2545	0
1 m-50 m	655,841,000	97.0145	0
1 m-100 m	659,485,000	98.7322	0
10 m-50 m	848,016,000	187.6014	0
10 m-100 m	843,021,000	185.2469	0
50 m-100 m	893,059,000	208.8336	0

P* <0.01 (α level of significance): The null hypothesis is rejected.

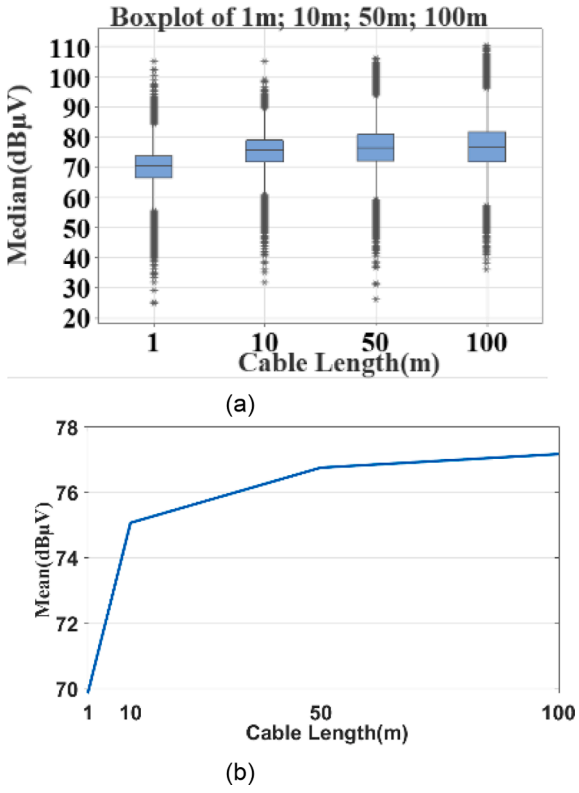

Fig. 7. Box(a) and Mains effect plot(b) for cable length.

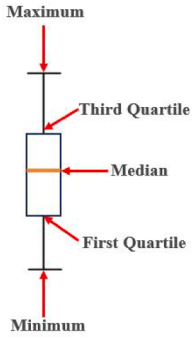

Fig. 8. Different parts of box plot.

length is higher. This is due to parasitic capacitances and CM mode current [28], which is proportional to cable length [29].

Figure 8 displays various statistical measures of the data, including the minimum, maximum, first quartile, third quartile, median, and outliers. The boxplot shows the range and quartiles, which provide information about the spread or dispersion of the data. The minimum and maximum values that exist in the dataset are shown by the lines extending from the box on either end, illustrating the range of values. The space between these lines is referred to as the range. It helps to find out how widely the data values vary.

Different parts of box plot is explained as following.

Maximum: The highest value found in the provided dataset.

Minimum: The highest value found in the provided dataset.

First Quartile: This is the value that separates the first quarter, or 25% of the dataset, from the rest.

Third Quartile: This is the value that separates the first three quarters, or 75% of the dataset, from the rest.

Median: The middle value in a dataset that divides it into two equal parts is the median, also known as the second quartile. The midpoint of the data distribution is represented by this central tendency measure.

According to Figure 7, which was indicated before, the maximum emission value for a cable length of 100 m is 110 dBuV, while the minimum emission value is 25 dBuV, resulting in a difference of around 85 dBuV between them. This is brought on by the switching-related emissions' tendency for amplitude variability.

3.2. *Impact of filter for EMI*

EMI filters are critical in reducing electromagnetic interference in three-phase applications, preventing interference, and ensuring compliance with EMC regulations. To understand the effect of drivers, the same model drivers were used. In this section, the noise levels of two drivers were compared to evaluate their noise suppression capabilities based on suggested standards. The primary objective was to determine the maximum electromagnetic interference conducted by the drivers. Additionally, the purpose of this section was to investigate the impact of EMI filters on the drivers and to determine whether a driver equipped with a filter could effectively suppress frequencies ranging from 9 kHz to 150 kHz. When the ASD-1 and ASD-2 drivers were linked to Motor-1 and Motor-2 with 100 m cable length independently, it was discovered that

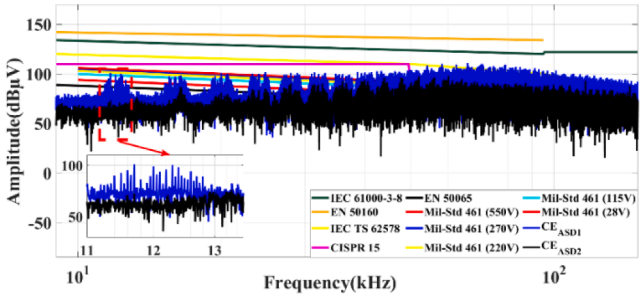

Fig. 9. EMI filter driver effect over CE.

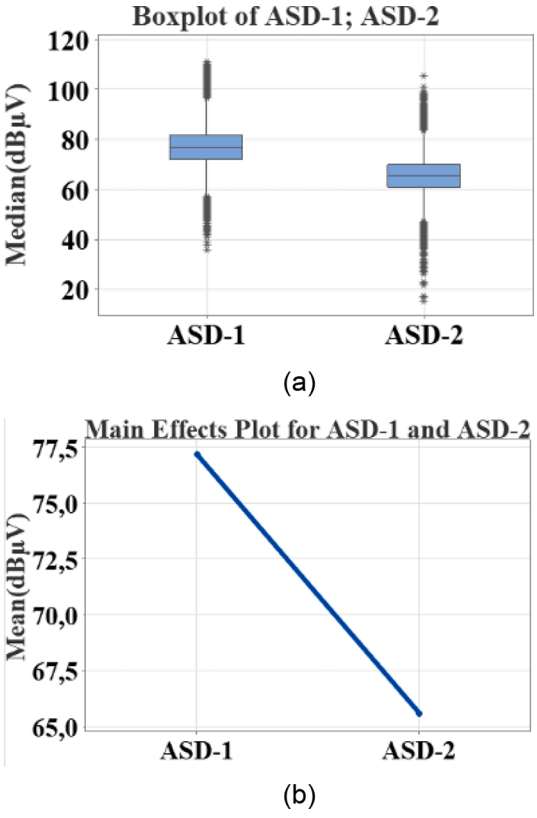

Fig. 10. Box(a) and Mains effect plot(b) for ASD-1, ASD-2.

ASD-1 did not have an EMI filter, as seen in Figure 9. CE for ASD-1 exceeds CISPR 15, EN 50065, and MIL-STD standards. CE for ASD-2 exceeds MIL STD and EN 50065 standards.

Although ASD 2 has an EMI filter (driver 1 exhibits lower levels of noise than driver 2, then it is likely that the driver has a filter). The findings revealed that if a driver had a filter, it would require redesigning to adequately suppress frequencies in the 9 kHz to 150 kHz range, and a filter redesign is suggested to meet the suggested standard limits. Furthermore, considering the results obtained, the driver was selected based on the worst conducted electromagnetic interference, and all measurement uncertainty evaluations were performed using this selected driver. This result is also supported by statistical tests illustrated in Figure 10.

3.3. Multiple converters operation impact over CE

Different converters may be linked to the system simultaneously in industrial applications. This section presents how the emissions vary when different converters are connected to the system. Two different types of mitigation were observed. A nonfiltered driver was used with a 100 m cable in the first sub-section (ASD-1), and then a filtered converter was tied parallel with a cable length of 50 m (ASD-1 + ASD-2) for the worst-case scenario. In both conditions, CE exceeds standards except for IEC 61000–3-8, EN 50160, and IEC TS 62578. CE is produced by power converters with a parallel topology increase, as seen in Figure 11 and Figure 12. However, this increase is not linear, according to Section 3.1 results.

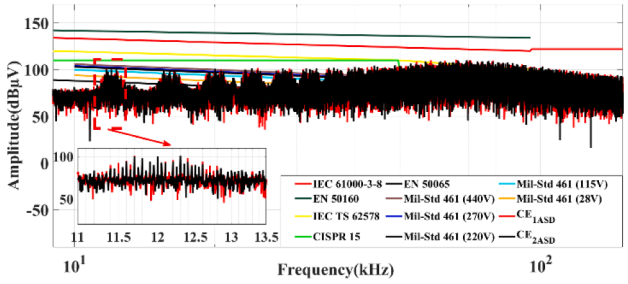

Fig. 11. Parallel converter's effect over CE.

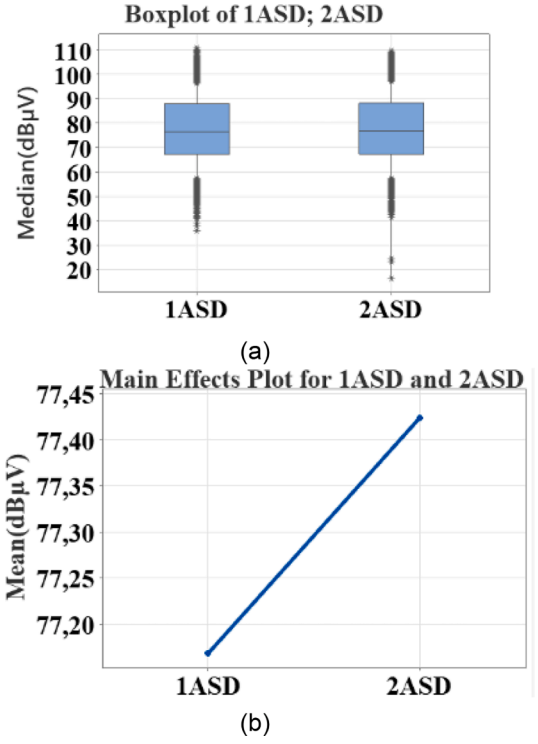

Fig. 12. Box(a) and Mains effect plot(b) for more than one converter.

3.4. The effect of cable assemblies

This section shows some examples of deviations by the varying manner of cable assemblies given in Figure 13 for the measurement uncertainty for conducted emission measurements. Figure 14 shows that the background noise is under the standard limits. Three methods of implementing meandering (cable layout-1, cable layout-2, and cable layout-3) are taken into consideration to present that the cable assemblies are essential: one bundled and tightened in the middle (Figure 13a), one tightly meandered around fixed positions on the ground plane (Figure13b) and one tightly coiled on the same board with a different style (Figure 13c). According to the results, CE exceeds EN 50065, MIL-STD (28 V), and MMIL-STD 115) standard limits. This exceeding has a considerable impact on performed emission results, as shown in Figure 14 and Figure 15.

The coupling works as a transformer due to the interference between cables. Magnetic fields through inductive coupling between cables have an impact on emissions [30]. According to the results, CE will decrease if cables meandered cable layout 3 style (Figure 13c). As a result, EMI will reduce with tightly meandered around fixed positions.

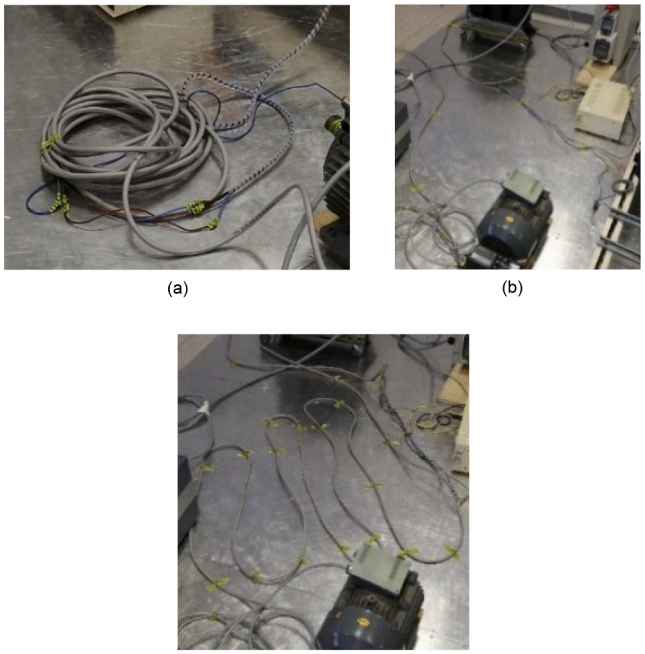

Fig. 13. Cable assemblies: layout-1 (a), layout-2 (b), layout 3- (c).

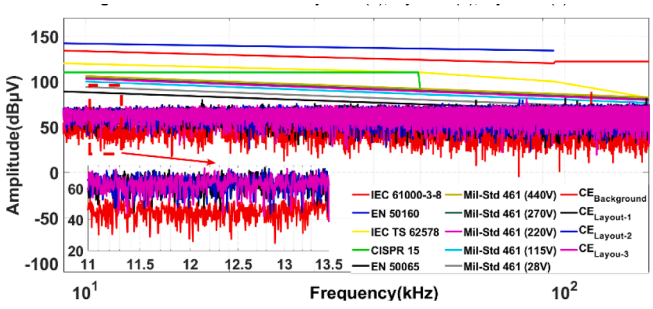

Fig. 14. Impact of cable assemblies' effect on CE.

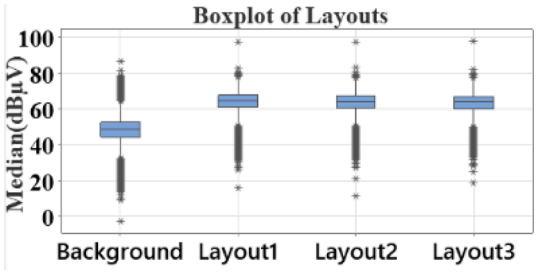

(a)

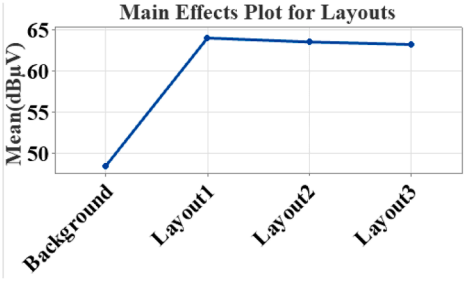

(b)

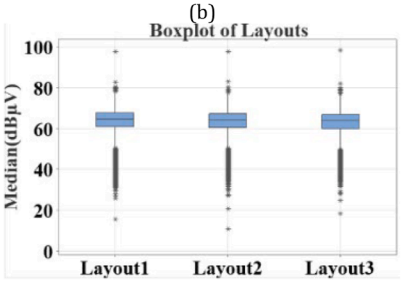

(c)

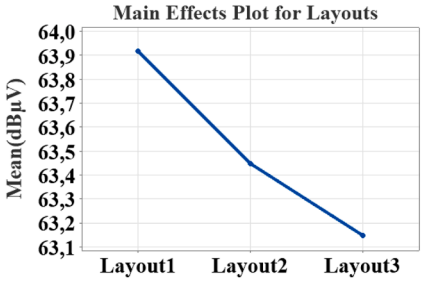

(d)

Fig. 15. Box (a),(c) and Mains effect plot(b),(d) of cable assemblies for four and three groups.

3.5. Various load effect

0.5 kW induction motor rig containing a powder brake was used to observe varying load conditions over the CE. The speed and current of the motor during the varying load tests are given in Table 4. Conducted emissions for different load levels are given in Figure 16 and Figure 17.

Table 4
Speed of motor under different torque.

Load(NM)	Speed(rpm)	Current(A)
0.04	1500	3.61
1	1499	3.7
2	1498	3.9
3	1497	4.2
4	1495	4.7
5	1494	5.3
6	1493	5.9
7	1490	6.5
8	1488	7.3

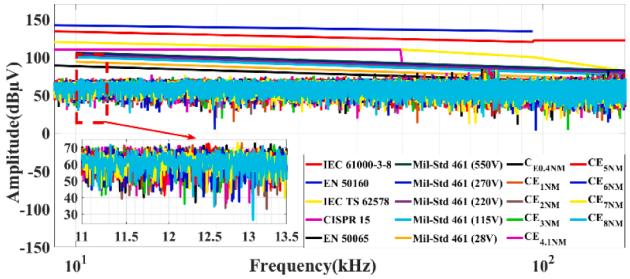

Fig. 16. Conducted emissions for different load levels.

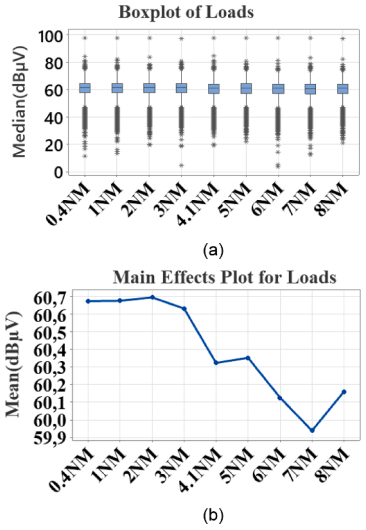

Fig. 17. Box(a) and Mains effect plot(b) for different load levels.

3.6. Speed of driver effect

This section presents an investigation of emission levels based on the frequency of the motor under no-load and load conditions. For the no-load condition mentioned in Section 3, Motor 1 and for load condition, Motor 3 were used with ASD-1 driver. In all speed conditions, CE exceeds EN 50065, MIL-STD (28 V), and MIL-STD D(115) standard limits, as seen in Figure 18 and Figure 19. Figure 18 and Figure 19 show no-load condition results. The presented results show that the value of the high-frequency harmonic components (kHz) in the current drawn by the driver from the network is more significant while starting the motor with low frequency, as the ratio of the harmonics below the fundamental and 50th harmonics. As the motor speed increases, the inverter can provide the necessary power with a lower ratio of high-frequency current, reducing the amount of EMI generated. This is because the motor's

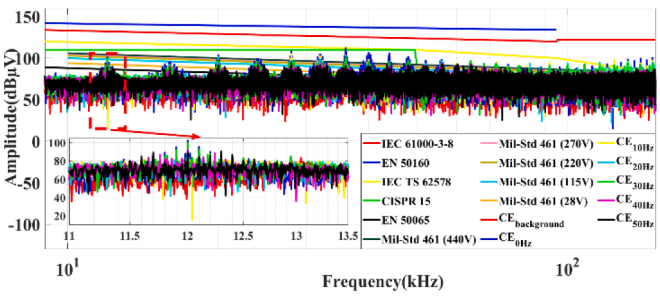

Fig. 18. Emission levels under no load and different frequency conditions.

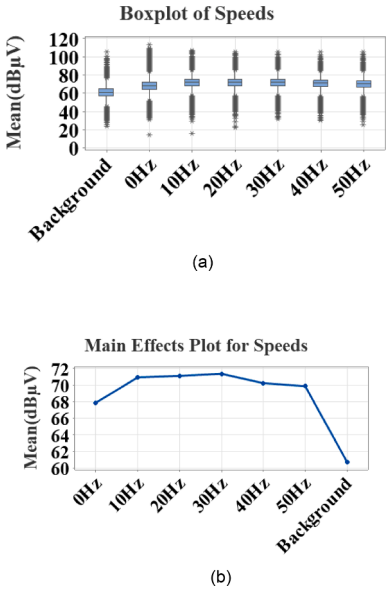

Fig. 19. Emission levels with Box (a) and Mains effect plot under ASD's frequency variations.

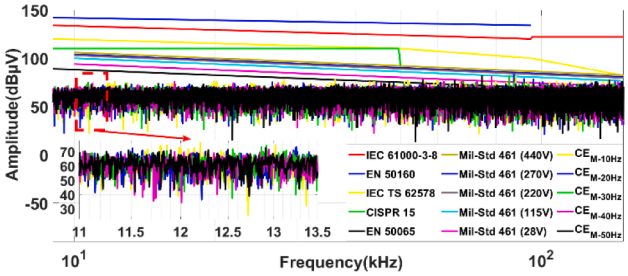

Fig. 20. Emission levels under load and different frequency conditions.

inductance starts to filter out the high-frequency components of the current, resulting in a lower overall noise level. Therefore, as the induction motor speed increases, the EMI generated by the inverter decreases due to the decrease in the ratio of high-frequency current. This is reflected in measured noise levels, which decrease as motor speed increases.

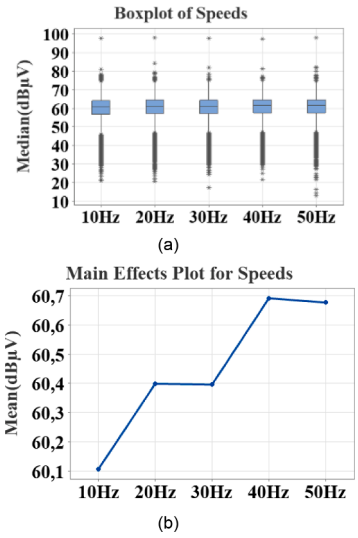

Fig. 21. Emission levels with Box (a) and Mains effect plot under ASD's frequency variations.

Additionally, the speed of the driver effect was investigated under the 8 Nm load condition to determine the worst-case scenario for a better filter design. The interesting thing happens when the motor's frequency increases, increasing the conducted emissions, as shown in Figure 20 and Figure 21. This indicated that torque significantly affects emission levels. Based on the information provided from experimental results, the worst operating scenario for conducted emissions appears to be when the system has a long cable, high driver speed, and no-load condition, with a circular meandering configuration. These factors can contribute to increased levels of conducted emissions, and designers need to consider them when designing power converters. Each high-frequency component within an electrical machine or device has high-frequency equivalent circuits leads to efficiency losses and increased heat generation. This can also, manifest as voltage fluctuations, frequency deviations, and other electrical disturbances. These issues can have a detrimental impact on the performance of connected devices, potentially leading to equipment failures or malfunctions. Therefore, an unloaded state with a maximum cable length, bundling and tightening the cables in the middle, along with the presence of high-speed drivers increases the degree of these effects. By addressing these issues early in the design process, it may be possible to prevent or minimize the impact of conducted emissions on the system's overall performance.

4. EMI filter design and element selection

EMI filter design method for a three-phase inverter circuit. For this, firstly, the simulation model of the system is created in the PSIM software to validate the filter design, as shown in Figure 22. The simulation consists of a DC-DC buck converter, three-phase DC-AC inverter, three-phase squirrel cage induction motor, LISN, EMI filter, and ground plane. The common parasitic mode capacitances of the converter are settled as Cm1- Cm10. CM and DM filter designs have been made in the PSIM environment. PSIM findings have also been passed to MATLAB software for filter parameter calculation. The simulation time step is 3.33 µsn to see the last frequency band, 150 kHz. Figure 23 compares the simulated and actual CE noise levels of the line and neutral conductors without design conduction.

The measured results and the results obtained from the simulation model match well and agree below 50 kHz. The discrepancy between the simulation model and the experimentally measured spectra above 50 kHz is caused by additional sources of interference, such as ambient and typical mode noises that are unknown since the driver inside is a black box. Thus, the results obtained from the simulation can also be utilized for the actual filter design steps. Since the worst-case scenario in the simulation occurred at maximum cable length, no load, and nominal speed, the filter design was made considering these conditions.

To evaluate the measurement uncertainty results obtained in the experimental environment, the behavior of CE at different cable lengths and load conditions has also been measured in the simulation environment.

The effect of cable length is given in Figure 24. As seen from the results, the switching frequency is 4 kHz, and the emission has also increased as the cable length increases.

The decrease in speed of the motor as it is loaded can lead to changes in the levels of CE. Simulating this scenario can provide useful information about the CE performance and compatibility of the motor. By evaluating the CE conditions when the motor is operating under different load conditions, it is possible to assess the impact of load changes on the CE level. As depicted in Figure 25 that as the load increases, the CE decreases. As seen from the results, the simulation results are consistent with the experimental results regarding measurement uncertainties. This indicates that the simulation environment provides a valuable tool for evaluating the EMI performance of a motor and predicting its behavior under different conditions.

The design steps are as follows.

Step 1: Firstly, the modelled of conducted emission comprises

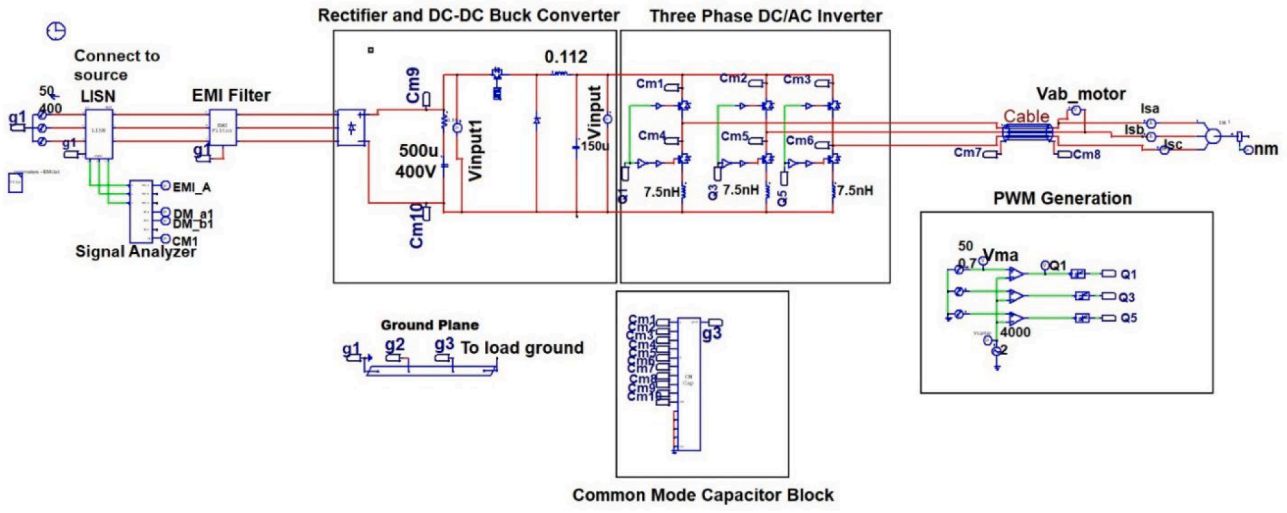

Fig. 22. Circuit frame of EMI filter and motor drive system.

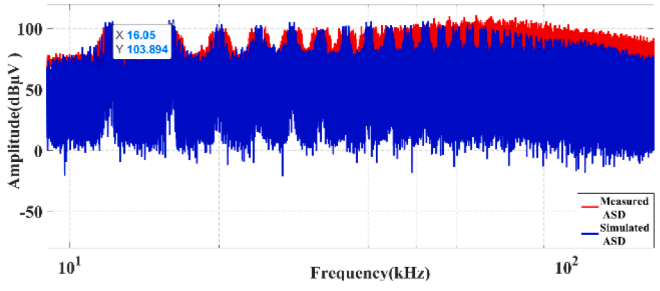

Fig. 23. The total conducted emissions were obtained from both the simulation and the receiver.

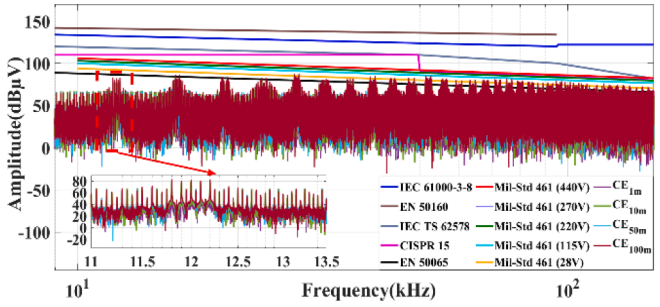

Fig. 24. EMI noise with various motor cable lengths in the PSIM environment.

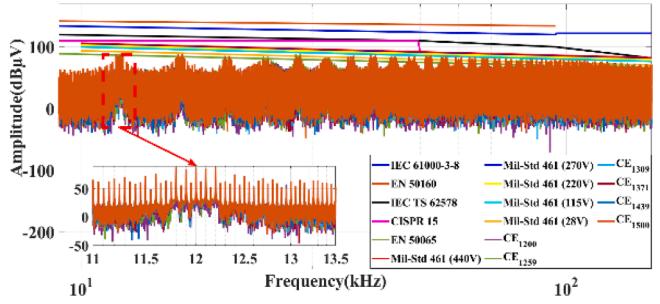

Fig. 25. Different load conditions on CE in the PSIM environment.

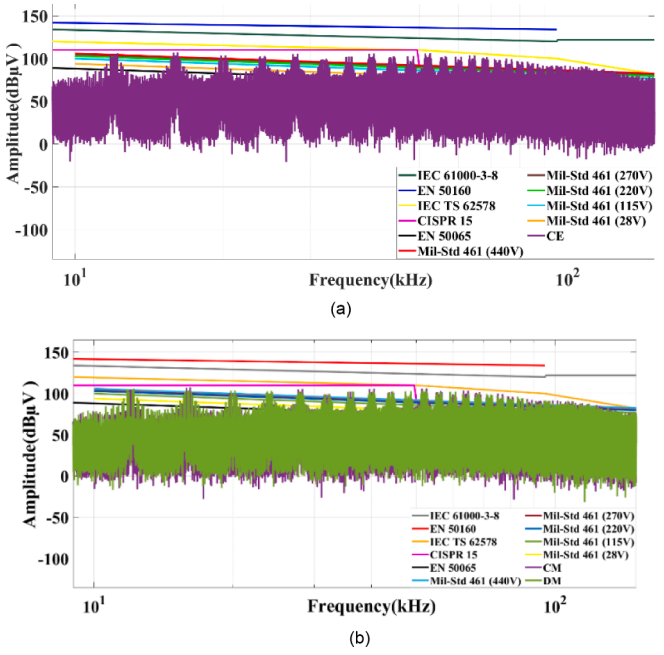

Fig. 26. EMI total noise (a) and CM-DM (b) noises result without filter.

standard limits covering a 9–150 kHz frequency range, as shown in Figure 26. EMI noise attenuation is required according to the results. The measurements of CM and DM noises are derived from the noise measurements of phase A and the neutral line. CM choke and Y capacitor for standard mode, the DM inductor, and X capacitors for differential mode are the components utilized in EMI filter design. Each filter element can potentially filter 20 dB/decade of noise [31–33]. The worst-case scenario (100 m cable length) recommended by the applicable standard has been considered. Filter topology and impedance mismatch concerns are considered throughout the filter design process [34]. The EMI filter input to be designed in this study is connected to an AC source, and after this connection, the point has a large C-valued capacitor against AC-DC voltage fluctuations. In other words, the output of the EMI filter is low impedance due to this capacitor. T-filter (LCL filter) has been selected as the filter topology since the EMI filter has low impedance at both ends.

Step 2: The CM and the DM attenuation requirements are determined using (1) and (2). EN-50065 is selected as the standard limit for required max attenuation. The noise attenuation must be 6 dB more than the exceeded noise because the measurements of DM or CM with the noise separator are higher than the actual value. Required CM and DM

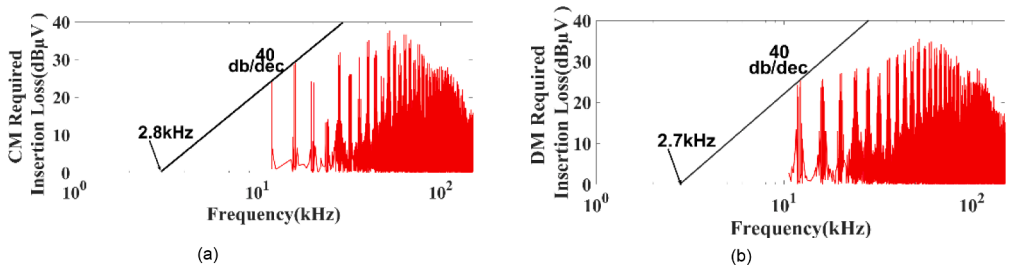

Fig. 27. Determining the required corner frequency based on CM and DM noise attenuation requirement.

attenuations and filter comer frequency are shown in Figure 27. The corner frequency is obtained by drawing a 40 dB/dec-slope line that is tangent to the required noise attenuation. According to the standard graphical method, the line's horizontal intercept determines the corner frequency. When the visual technique is performed to identify the corner frequency, cutoff frequencies are found as $f_{CM} = 9.3$ kHz for CM noise and $f_{DM} = 10.3$ kHz for DM noise, respectively. Figure 27 shows that a higher corner frequency would affect the size of the filter elements. Still, since the corner frequency is already below 50 kHz, the simulation results can be utilized for the actual filter design steps.

$$Vreq_{CM}(dB\mu V) = V_{CM} - Vlim_{EN50065} + 6 \quad (1)$$

$$Vreq_{DM}(dB\mu V) = V_{DM} - Vlim_{EN50065} + 6 \quad (2)$$

The equivalent circuit of per phase's EMI filter is given in Figure 28.

Step 3: CM components are common mode choke LCM and capacitance Cy: IEC 60950 safety organization states that the maximum leakage current value is limited to 3.5 mA for 50 Hz [35–36]. CY capacitance value should ensure the leakage current requirement and is calculated with Equation (3). According to the EN50160 standard, the grid voltage (400 V) unbalance is assumed to be 3% for calculating the leakage current. The tolerance value of the capacitors utilized in the filter design is 20% of the rated value. Therefore, Y capacitors are selected as 4.7 nF. Also, L_{CM} and 2Cy should have a resonance frequency determined in Step 2. Thus, L_{CM} is calculated with Equation (4). From (4), the calculated CM inductance is LCM 343.7 mH.

$$C_{Ymax} = I_{Leakage}/(1.1*U*2\pi f)$$

$$L_{CM} = (1/2C_Y)(1/2\pi f_{CM})^2 \quad (4)$$

Step 4: DM components are differential mode choke L_{DM} and capacitance Cx. Since a CM choke's leakage inductance can be used as a DM choke, separate DM chokes may sometimes not be required. In practice, leakage inductance is typically 0.5–2% of the LC value. As a result, L_{DM} is selected as 5.2 mH. C_X is related to L_{DM} through the specific frequency requirement for f_{DM} as seen in (5) and calculated as 0.62 μF.

$$C_X = (1/L_{DM})(1/2\pi f_{DM})^2 \quad (5)$$

Step 5: EMI noise was measured with a filter to verify the calculated parameter results. Compared to Figure 26 (before filtering), CM, DM, and total noise are decreased as seen in Figure 29. According to the simulation results, the filter meets the required attenuation. Therefore, the same procedure will be applied to the actual filter design.

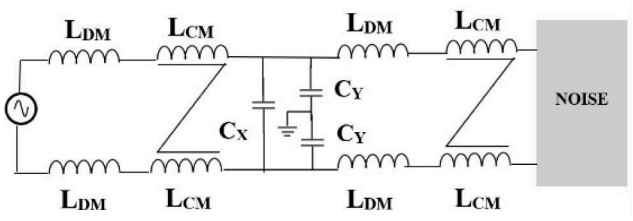

Fig. 28. The structure of the EMI filter (a), Equivalent circuit of CM (b) and DM (c) noise.

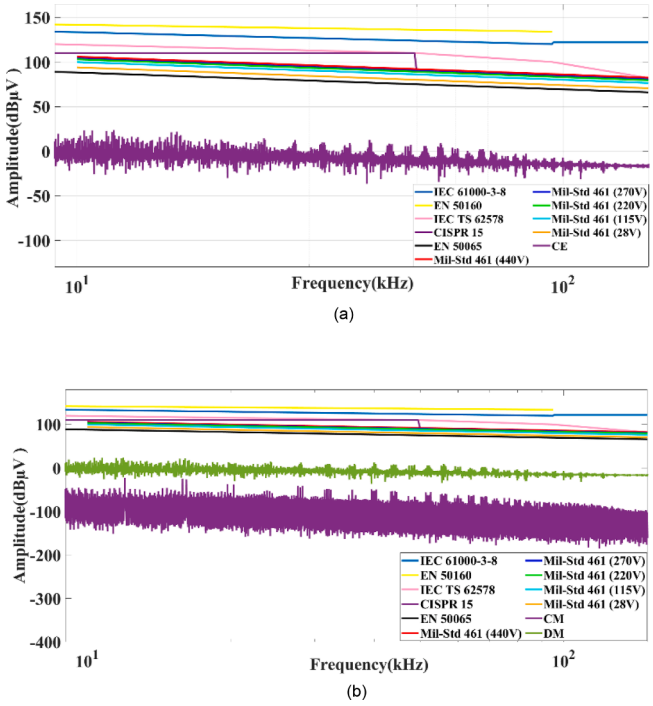

Fig. 29. Suppression of total (a) noise and CM-DM (b) noises.

5. Conclusion

An investigation was carried out into the uncertainty in three-phase conducted emissions measurements induced by various working circumstances in the 9–150 kHz frequency range band characterized by the LISN bandwidth. Because different standards groups are interested in the emission limitations for higher frequencies (2 kHz–150 kHz in this study, a limit standard was offered for this band range. A frequency domain analysis statistical approach is used to validate the measurement results for EMI noises. The observed CE results with and without the EMI filter exceed the suggested CE limits. To eliminate EMI, filter engineers must design filters effectively for this product. For an effective functional design, engineers need to initially understand how EMI is produced in the converter. This paper provides a big picture concerning uncertainty about conducted emissions, including cable length, manner of meandering, speed of the motor, and torque. In this investigation, the findings are listed below.

As cable length increase, expected mode noise increase with the cable capacitive effect. So, excessive cable length must be short as soon as possible. Thus, the short cable will reduce EMI.

The cable of meandering affects inductive coupling. EMI decreases with tightly meandering around set points (cable layout 3).

Output frequency of the ASD-1 concerns variations in emissions level. While the output frequency of ASD-1 increases under no load condition, EMI decrease. The ratio of the harmonics below the fundamental and the 50th harmonic led to this. One interesting takeaway is that the loaded scenario is the opposite. Experimental results demonstrate that braking torque applied to the motor impacts the noise level. EMI disturbance reduces in the highest load condition.

- Most studies used just one standard limit level associated with ASD drivers and mostly above 30 MHz frequency. But, this study focuses on the under 150 kHz frequency range because of the gap in this frequency range.
- There was no analysis with the statistical approach in terms of the influence of cable length, manner of cable, speed of the motor, and torque. Thus, the emission levels were depicted more accurately with this work.
- Studies on conducted emissions of adjustable three-phase speed drivers focus on just one uncertainty. But, this study represents all aspects of the uncertainty of the measurement system. Here, the filter design was made based on the worst-case scenario: the unloaded state with a maximum cable length of 100 m in the simulation. Also, the 9–150 kHz frequency part of the design specification gives a quick filter design that at least meets the lowest suggested standard limit. The same procedure can be extended to the filter, and this work will guide EMI designers in future works. Considering measurement uncertainties in EMI filter design is crucial to ensure the filter's performance is at the desired level in real-world conditions. Therefore, designing the filter based on worst-case scenarios can make the filter performance more reliable against variations. Another critical aspect of innovation is designing the filter to meet the recommended standard limits in the 9–150 kHz band. This frequency band is where electromagnetic noise generated and transmitted by many electronic devices is prevalent, and thus, the filter's good performance in this band is critical for many applications. However, it is essential to consider measurement uncertainties in filter design to ensure that the design complies with the specified standards. Ignoring measurement uncertainties can result in the design failing to perform as expected in real-world conditions.

Declaration of Competing Interest

The authors declare that they have no known competing financial interests or personal relationships that could have appeared to influence the work reported in this paper.

Acknowledgments

This work was supported in part by Ondokuz Mayis University under Projects PYO.MUH.1904.21.011 and PYO.MUH.1906.21.002

References

[1] G. Betta, D. Capriglione, G. Tomasso, Evaluation of the measurement uncertainties in the conducted emissions from adjustable speed electrical power drive systems, IEEE Trans. Instrum. Meas. 53 (4) (2004) 963–968, https://doi.org/10.1109/TIM.2004.830586.
[2] A. Safayet, M. Islam, Modeling of conducted emission for a three-phase motor control inverter, IEEE Trans. Ind. Appl. 57 (2) (2021) 1202–1211, https://doi.org/10.1109/TIA.2021.3052744.
[3] B. Revol, J. Roudet, J.L. Schanen, P. Loizelet, EMI study of three-phase inverter-fed motor drives, IEEE Trans. Ind. Appl. 47 (1) (2011) 223–231, https://doi.org/10.1109/TIA.2010.2091193.
[4] Texas Instruments. AN-2162 Simple Success with Conducted EMI from DC-DC Converters. ti.com, 2012.
[5] R. J. Hijmans, J. van Etten. Raster: Geographic Analysis and Modeling with Raster Data. R Package Version 2.0-12. http://CRAN.R-project.org/package=raster, 2012.
[6] M.L. Heldwein, J. Biela, H. Ertl, T. Nussbaumer, J.W. Kolar, Novel three-phase CM/DM conducted emission separator, IEEE Trans. Ind. Electron. 56 (9) (2009) 3693–3703, https://doi.org/10.1109/TIE.2009.2025287.
[7] C. Leroi, Conducted Disturbances in the Frequency Range 2–150 kHz: Sources and Propagation, Luleå University of Technology (2021). Ph.D. dissertation.
[8] D. Ritzmann, S. Lodetti, D. de la Veg, V. Khokhlov, A. Gallarreta, P. Wright, J. Meyer, I. Fernandez, D. Klingbeil, Comparison of measurement methods for 2–150-kHz conducted emissions in power networks, IEEE Trans. Instrum. Meas. 70 (2021) 1–10.
[9] L. Sandrolini, D. W. P. Thomas, M. Sumner, C. Rose, Measurement and evaluation of the conducted emissions of a DC/DC power converter in the frequency range 2–150 kHz, Proc. 2018 IEEE Symp. Electrom. Comp., Signal Integrity and Power Integrity (EMC SI & PI), Long Beach, CA, USA 2018, pp. 345-350, https://doi.org/10.1109/EMCSI.2018.8495199.
[10] D. Ritzmann, S. Lodetti, D. de la Vega, V. Khokhlov, A. Gallarreta, P. Wright, D. Klingbeil, Measurement of 2–150 khz conducted emissions in power networks, Proc. Conf. Precision Electromagn. Meas., Denver, CO, USA, 2020, pp. 1-2. https://doi.org/10.1109/CPEM49742.2020.9191695.
[11] A. D. Khilnani, A. E. Pena-Quintal, E. Ballukja, M. Sumner, D. W. Thomas, L. Sandrolini, A. Mariscotti, Influence of impedance interaction & comparability on spectral aggregation (2–150 kHz) in DC grids, 2022 International Symposium on Electromagnetic Compatibility–EMC Europe, Gothenburg, Sweden, 2022, pp. 788-792.
[12] S. Lodetti, A. Gallarreta, D. Ritzmann, V. Khokhlov, P. Wright, J. Meyer, I. Fernández, D. de la Vega, On the suitability of the CISPR 16 method for measuring conducted emissions in the 2–150 kHz range in low voltage grids, Electric. Power Syst. Res. 216 (2023) 109011.
[13] Cenelec. Study Report on Electromagnetic Interference Between Electrical Equipment/Systems in the Frequency Range below 150 kHz. Irish Standard Recommendation, 2013.
[14] P. A. Beeckman, The influence of positioning tables on the results of radiated EMC measurements, 2001 IEEE EMC International Symposium, Symposium Record. International Symposium on Electromagnetic Compatibility (Cat. No.01CH37161), Montreal, QC, Canada, 2001, pp. 280-285, https://doi.org/10.1109/ISEMC.2001.950635.
[15] L. Van Wershoven, The effect of cable geometry on the reproducibility of EMC measurements, Int. Symp. Electromagnetic Compatibility, Seattle, WA, USA,1999, pp. 780-785, https://doi.org/10.1109/ISEMC.1999.810118.
[16] J. Pahl, Conducted Emissions of Low Power Variable Speed Drives, Metropolia University of Appl. Sci. (2020). Bachelor's thesis.
[17] S.A. Pignari, A. Orlandi, Long-cable effects on conducted emissions levels, IEEE Trans. Electromagn. Compat. 45 (1) (2003) 43–54, https://doi.org/10.1109/TEMC.2002.808023.
[18] B. Benazza, A. Bendaoud, J.L. Schanen, Influence of cable lengths on EMI emissions of a DC/DC converter influence of cable lengths on EMI emissions of a DC/DC converter, Modeling, Measurement and Control A 93 (2020) 26–30, https://doi.org/10.18280/mmc_a.931-404.
[19] M. Richard, Cable bundling, The EMC Journal 71 (2007).
[20] V. D. Santos, N. Roux, B. Revol, B. Sareni, B. Cougo, J. -P. Carayon, Unshielded cable modeling for conducted emissions issues in electrical power drive systems, 2017 International Symposium on Electromagnetic Compatibility - EMC EUROPE, Angers, France, 2017, pp. 1-6, https://doi.org/10.1109/EMCEurope.2017.8094736.
[21] M. Moreau, N. Idir, P. Le, Moigne, Modeling of conducted EMI in adjustable speed drives, IEEE Trans. Electromagn. Compat. 51 (3) (2009) 665–672, https://doi.org/10.1109/TEMC.2009.2025269.
[22] D. Gallo, C. Landi, N. Pasquino, V. Ruotolo, About measurement uncertainty of conducted emissions generated by a variable speed drive, 10th IMEKO TC4 International Workshop on ADC Modelling and Testing, 2005.
[23] J. Luszcz, Motor cable effect on the converter fed AC motor common mode current, Proc. 7th Int. Conf. Workshop Compat. Power Electron, Tallinn, Estonia, 2011, pp. 445-450, https://doi.org/10.1109/CPE.2011.5942277.
[24] H. Hizarci, U. Pekperlak, U. Arifoglu, Conducted emission suppression using an EMI filter for grid-tied three-phase/level T-type solar inverter, IEEE Access 9 (2021) 67417–67431, https://doi.org/10.1109/ACCESS.2021.3077380.
[25] Y. Maillet, L. Rixin, W. Shuo, F. Wang, R. Burgos, D. Boroyevich, High-Density EMI Filter Design for DC-Fed Motor Drives, IEEE Trans. Power Electron. 25 (5) (2010) 1163–1172.
[26] Electromagnetic Compatibility. General guide on harmonics and interharmonics measurements and instrumentation. IEC Standard 61000-4-7. 1997.
[27] T. Karaca, B. Deutschmann, G. Winkler, EMI-receiver simulation model with quasi-peak detector, IEEE Int. Symp. Electromagn. Compat., Dresden, 2015, pp. 891–896.
[28] CTC AppNotes. Cable Length Calculation for Hazardous Locations. https://ctconline.com/media/ehlacmb2/5-13.pdf, 2022.
[29] W.L. de Souza, H. de Paula, A. De Conti, R.C. Mesquita, Cable parameter calculation for typical industrial installation methods and high-frequency studies, IEEE Trans. Ind. Appl. 54 (4) (2018) 3919–13392, https://doi.org/10.1109/TIA.2018.2811382.
[30] S. Kong, B. Bae, D. H. Jung, J. J. Kim, S.Kim, j. Kim, Investigation of electromagnetic radiated emission and interference from multi-coil wireless power transfer systems using resonant magnetic field coupling, IEEE Transactions on Microwave Theory and Techniques, 63.3 (2015) 833-846, https://doi.org/10.1109/TMTT.2015.2392096.
[31] L. Ensini, L. Sandrolini, D. W. P. Thomas, M. Sumner, C. Rose, Conducted emissions on DC power grids, 2018 International Symposium on Electromagnetic Compatibility (EMC EUROPE), Amsterdam, Netherlands, 2018, pp. 214-219, https://10.1109/EMCEurope.2018.8485174.
[32] Z. Wang, Conducted EMI Noise Prediction and Filter Design Optimization, Virginia Tech (2018). Ph.D. dissertation.

[33] S. Fu-Yuan, D.Y. Chen, W. Yan-Pei, C. Yie-Tone, A procedure for designing EMI filters for AC line applications, IEEE Trans. Power Electron. 11 (1) (1996) 170–181, https://doi.org/10.1109/VPPC.2008.4677781.
[34] A. Mariscotti, Harmonic and superharmonic emissions of plug-in electric vehicle chargers, Smart Cities 5 (2) (2022) 496–521, https://doi.org/10.3390/smartcities5020027.
[35] B. Narayanasamy, Impedance mismatching based design of passive and active EMI filters for power converters, The Ohio State University (2016). Ph.D. dissertation.
[36] I. Manushyn, Design and Optimization of EMI Filters for Power Electronics Systems, Technische Universität Darmstadt, 2019, M.S. thesis.